$^{10}B(n,\alpha)^7Li$, $^7Li^*$ differential cross section measurements between 0.2 and 1.25 MeV†

R. M. Sealock and J. C. Overley
Physics Department, University of Oregon, Eugene, Oregon 97403
(Received 8 December 1975)

α-particle yields from the $^{10}B(n,\alpha)^7Li, ^7Li^*$ reactions have been measured at eight angles between 0° and 150° for neutron energies between 200 and 1250 keV. A thick natural lithium target bombarded by a pulsed proton beam provided a neutron-energy continuum. α particles from the two reactions were distinguished by measuring the sum of α-particle and neutron flight times as well as α-particle energies. Yield data were converted to c.m. differential cross sections and each angular distribution was fitted with a series of Legendre polynomials. Coefficients of the P_0 terms are compared with other measurements. The coefficients of the higher order terms are qualitatively interpreted in terms of the level structure of ^{11}B.

[NUCLEAR REACTIONS $^{10}B(n,\alpha_0)$, $^{10}B(n,\alpha_1)$; $E=0.2$–1.25 MeV, measured $\sigma(\theta)$.]

I. INTRODUCTION

For neutrons with energies less than 1.5 MeV incident on ^{10}B, ^{11}B compound nuclei may be formed with excitation energies between 11.456 and 12.8 MeV. The primary decay modes at these energies are α-particle and neutron emission. For α decay, the residual ^7Li nucleus can be left in either its ground state or its first excited state. The Q values for the $^{10}B(n,\alpha_0)^7Li$ and $^{10}B(n,\alpha_1)^7Li^*$ reactions are 2.792 and 2.314 MeV,[1] respectively. At thermal energies the (n,α_1) reaction is dominant with a cross section of 3599 b (Ref. 2); the (n,α_0) reaction cross section is 242 b.[2] The cross section for each reaction has a $1/v$ dependence up to a neutron energy of about 100 keV.[3] At higher energies several broad states cause departure from the $1/v$ dependence.

Other neutron induced reactions in this energy range are (n,p), (n,t), and (n,γ). Their cross sections are sufficiently small that the total neutron absorption cross section has been approximated by the sum of the (n,α_0) and (n,α_1) cross sections.[4]

These properties of the reaction make ^{10}B suitable for neutron absorption, detection, and flux standardization. As a result there have been many measurements of the absorption cross section,[3-9] the (n,α_0) and (n,α_1) integrated cross sections,[10-12] and the α_0/α_1 branching ratios.[5,9,10,13-16] These quantities have been studied from thermal energy to several MeV, although most measurements are below 500 keV. Above 100 keV there are significant disagreements among the various measurements. For example, the (n,α_1) integrated cross sections of Davis *et al.*[11] and those of Nellis, Tucker, and Morgan[12] differ by almost a factor of 2 near 1 MeV. Measurements in the 100-500 keV range commonly disagree by more than their quoted errors. Differing shapes for (n,α) excitation curves obtained in these studies has led to uncertainty about the level structure of ^{11}B.

States in ^{11}B have also been studied by the inverse reaction, $^7Li(\alpha,n)^{10}B$,[10,17] and by $^7Li(\alpha,\alpha)^7Li$ and $^7Li(\alpha,\alpha_1)^7Li^*$ scattering measurements.[18] Elastic scattering and analyzing power measurements for the $^{10}B(n,n)^{10}B$ reaction have been made.[19] Recently much of this information has been combined in multichannel R-matrix calculations.[19,20] The $1/v$ behavior of the (n,α) cross sections is now identified mainly with a broad s-wave $\frac{7}{2}^+$ resonance at a neutron energy of about 0.37 MeV.[19] It appears that five or more states affect the (n,α) cross sections below 1.5 MeV. They have energy separations about equal to their widths (100–200 keV) and some have undetermined spin and parity.

Differential (n,α) cross sections are presently available only for the ground state reaction by applying detailed balance to $^7Li(\alpha,n)^{10}B$ angular distributions.[17] Because of the practical value of such cross sections, Lane[21] and his co-workers have made predictions of (n,α) angular distributions. These were calculated from ^{11}B parameters obtained in their R-matrix calculations. Since differential cross sections would allow R-matrix techniques to more accurately determine properties of the $A=11$ system, we have measured them for neutron energies from 0.2 to 1.25 MeV.

This experiment is part of a continuing effort using the University of Oregon 5 MV Van de Graaff accelerator to study neutron induced reactions.[22,23] The measurements use pulsed beam and "white" neutron source techniques. A neutron-energy continuum is produced via $^7Li(p,n)^7Be$ reactions in a

thick lithium target. The pulsed proton beam allows separation of α_0 and α_1 particles of the same energy by measurements of neutron flight times. Reaction yield data are sorted as a function of flight time and particle energy. Experimental details have been described at length in a paper on a similar study[23] of the ^{6}Li$(n, t)^4$He reaction. Geometrical calculations required by the use of relatively large solid angles and thick neutron source targets have also been previously reported.[24] The present paper contains a summary of the experimental details and data reduction processes and discusses the results of the measurement.

II. EXPERIMENTAL DETAILS

The neutron continuum was produced by a pulsed proton beam, focused to a 2 mm spot, striking a thick natural lithium target. The beam had a pulse repetition period of 500 nsec and pulse widths of about 1.2 nsec, full width at half maximum. Several beam energies in the 2.5 to 3.25 MeV range were used and typical time averaged beam currents were 5 μA. Neutron spectra were measured by the time-of-flight techniques used in this laboratory by Burke, Lunnon, and Lefevre[25] for studying ^{7}Li$(p, n)^7$Be thick target neutron yields. We used the detector, biasing techniques, and detection efficiencies of Ref. 25 to determine effective yields for our experimental configuration. Yields were slightly different from those in Ref. 25 due to using a different lithium target holder, different proton energies, and attenuation of the incident neutrons by our target chamber. Time-of-flight spectra from the ^{7}Li$(p, n)^7$Be reaction were measured and converted to energy spectra for each of the incident proton energies used.

An evacuated chamber containing the ^{10}B target and a silicon surface barrier detector was placed at 0° relative to the proton beam. The target chamber was designed with minimal mass near the ^{10}B target to reduce the effects of scattered neutrons. Targets were thin films of isotopically enriched boron that had been evaporated onto tantalum substrates. The detectors were totally depleted and typically 200 μm thick and 150 mm^2 in active area. For some data runs a polyethylene neutron attenuator was used to shield the detector from the neutron source. The edge of the attenuator facing the neutron flight path was shaped so that neutrons from the source target could not scatter from any surface into the ^{10}B target. Although it raised the background, a reduction in detector damage by fast neutrons resulted.

Both flight time and particle energy were derived from the detector output. A fast timing signal, derived from the preamplifier output pulse by a constant fraction timing discriminator, was used to start a time to amplitude converter (TAC). An amplified and delayed pulse from a ferrite-core beam pulse pickoff provided a stop signal. A biased amplifier connected to the TAC output was used to select a flight time window about 30 nsec wide. The biased amplifier output was routed to one input of a dual analog-to-digital converter (ADC). The other input of the ADC received amplified linear signals from the detector. Both ADC outputs were stored by an on-line PDP-7 computer programmed to create a 32×128 channel array of counts as a function of flight time and particle energy. Events with flight times inside the flight time window were stored in time channels 2 through 32. Events with flight times either too long or too short were stored in the first time channel.

A precision pulser which had been calibrated against α particles from a thin ^{241}Am source was used for linearity checks and setting energy channel widths. Pulser outputs corresponding to known energies were routed through the electronics to the appropriate ADC input. Peaks in the resulting pulse height spectrum were least squares fitted by a linear equation to obtain the energy scale. Delay techniques were used to determine the slope of a linear time scale. The time scale intercept was calculated in a least squares fit to a set of channels taken from the (n, α) data. These channels were visually estimated high energy edges of the loci within which counts of interest were stored.

Figure 1 shows raw data, excluding the first time channel, that were collected at a laboratory angle of 60° over a period of about 15 hours. Diameters of the dots are approximately proportional to the number of counts per channel. The solid lines are calculated limits of the α-particle loci and will be discussed later. Counts due to ground state α particles are stored in the higher energy locus and the α_1 locus is the lower energy one. Loci for the ^{7}Li and ^{7}Li* nuclei are barely distinguishable near the left edge of the figure between time channels 10 and 20. It was impossible with our experimental configuration to separate ^{7}Li and ^{7}Li* counts from each other or from background.

Because the difference between the (n, α_0) and (n, α_1) Q values is small compared to either Q value, the α-particle loci are not always well separated. Loci widths result from α-particle energy loss in escaping the target, kinematic broadening, and resolution factors. In this experiment overlap of the loci is primarily determined by the target thickness and solid angles. Since kinematic broadening varies with angle, it was possible to keep the run time under one week for a set of angular distributions by choosing dif-

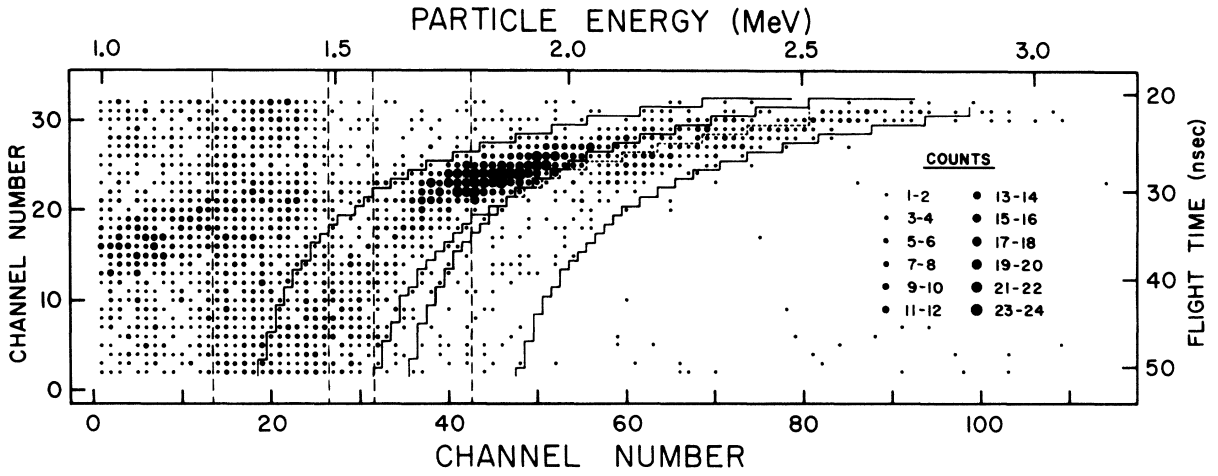

FIG. 1. A representation of raw data. The diameters of the dots are approximately proportional to the number of counts per channel. These data were taken at a nominal reaction angle of 60° with a 105 $\mu g/cm^2$ thick target. The integrated proton beam current was 250 mC. Calculated limits of the α-particle loci are shown by the solid lines. The dashed lines indicate regions where $^{10}B(n,\alpha)^{7}Li$ reactions due to room thermalized neutrons contribute to the background.

ferent neutron flight paths and target and detector radii for each angle. For various sets of geometrical parameters, anticipated locus limits and solid angles were calculated. Those parameters were chosen which gave the best compromise for minimum running time, detector damage, and background and maximum count rate and separation of loci.

The ^{10}B content of the targets was studied by α-particle yield comparisons between ^{10}B targets and a ^{6}LiF target of known composition. A therma_ neutron flux was created by placing a 10 cm thick polyethylene slab between the neutron source and target chamber. Measured energy spectra contained peaks due to α particles from the $^{6}Li(n,t)$-^{4}He and $^{10}B(n,\alpha)^{7}Li$ reactions. A target purity factor, defined as the fraction of the energy loss thickness due to ^{10}B atoms, was calculated from the energy loss thicknesses (full width at half maximum peak widths) and integrated counts after background subtraction. Known stopping cross sections, thermal neutron cross sections, and ^{6}LiF target composition were used in the calculation. It was assumed that stopping cross sections for the contaminants had the same energy dependence as that for ^{10}B over the energy range of interest. Measured target purity factors were used in the data analysis to calculate effective stopping cross sections per ^{10}B atom for each target. Most of the data were taken with a 105 $\mu g/cm^2$ thick target which had a purity factor (0.913) in good agreement with an isotopic analysis of the target material before evaporation (94.3 at.% ^{10}B).

Figure 1 shows that for some energies the counts of interest are nearly lost in background. There are two major sources of background within the data loci. γ rays are produced by (p,γ) reactions in the beam tube and (n,γ) reactions in and near the detector. Since γ rays deposit energy in the detector primarily by Compton scattering, this background has a smooth energy dependence. Room thermalized neutrons produce α-particle background by the $^{10}B(n,\alpha)^{7}Li$ reactions. These events have no time correlation with the beam pulse. As a result they are stored in the first time channel and in two vertical bands whose widths indicate the target thickness. These bands are shown in Fig. 1 by the dashed lines. The band due to α_0 events always crosses the α_1 data locus. For back angles the α-particle energy can be less than that from thermal neutron breakup and thus each band can cross its corresponding data locus.

Data were collected for two sets of angular distributions. An initial run used 85 and 105 $\mu g/cm^2$ thick targets, incident proton beam energies of 3.0, 3.18, and 3.25 MeV, and angles of 0°, 30°, 55°, 90°, 125°, and 150°. For a second run all data were taken with the 105 $\mu g/cm^2$ thick target and a 3.0 MeV beam energy giving a maximum neutron energy of 1.3 MeV. In this case angles of 60° and 120° were used rather than 55° and 125°. The polyethylene detector shield was used at 30°, 55°, 60°, and 90°. Neutron flight paths ranged from 12 to 20 cm and the charged particle flight path was 11 cm. The effective target area was defined by circular masks of 0.6 to 1.25 cm radius.

Because of high backgrounds two supplementary runs were made to improve statistical accuracy for the 120° and 150° cross sections below 500 keV neutron energy. In one case a reduced beam energy (2.5 MeV) was used, resulting in slightly less background due to the lower total number of neutrons. A second method yielded the best low energy, back angle data. A beam energy of 3.0 MeV was used with a short neutron flight path (8 cm), a 1.5 cm target radius, and correspondingly large solid angles. Although the counts to background ratio was not improved, the larger yield allowed the counts of interest to be more accurately separated from background. Overlap of the loci was too severe to determine cross sections from this run for neutron energies above 500 keV.

III. DATA ANALYSIS

The loci widths and the use of an incident neutron continuum create unusual problems in converting reaction yields to cross sections. An approximate technique for the analysis of such data is discussed in Ref. 24, where expressions for differential cross sections and average geometrical parameters with standard deviations are presented. The differential cross section $\sigma(\bar{E}_n, \bar{\mu})$ at a mean neutron energy $\bar{E}_n$ and mean reaction angle cosine $\bar{\mu}$ is

$$\sigma(\bar{E}_n, \bar{\mu}) = \frac{Y\epsilon(\bar{E}_\alpha)}{I(\bar{E}_n, \bar{\nu})(\Delta E_n \Delta E_\alpha)\Delta\Omega} \quad . \tag{1}$$

In this expression $\epsilon(\bar{E}_\alpha)$ is the effective stopping cross section per ^{10}B atom at an average α-particle energy $\bar{E}_\alpha$, and $I(\bar{E}_n, \bar{\nu})$ describes the number of neutrons per steradian incident on the ^{10}B target as a function of neutron energy at an average neutron emission angle cosine $\bar{\nu}$. Effects of extended geometry are included in the solid angle convolution $\Delta\Omega$. Target thickness effects are included in the factor $\Delta E_n \Delta E_\alpha$, which is an area in a neutron-energy–particle-energy space centered on $\bar{E}_\alpha$ and $\bar{E}_n$. It is related to the area in the flight-time–particle-energy space from which the reaction yield Y is obtained.[24]

The first step in the analysis is to determine the expected loci of counts. For a given energy channel number the range of α-particle energies produced in the reaction is calculated from the energy calibration and the α-particle energy loss in the target. Corresponding neutron energy and flight time limits are calculated through nuclear reaction kinematics from mean geometrical parameters plus and minus their standard deviations. The time limits are increased by the timing resolution, converted to flight time channel numbers, and rounded off to integral channel numbers. Typical results of this computer calculation are illustrated by the solid lines in Fig. 1.

The next step is to correct the number of counts per channel within the loci for background. The energy spectrum corresponding to the first time channel is used to estimate background. This is the sum of α_0 and α_1 peaks due to thermal neutron breakup and a γ-ray spectrum that decreases approximately exponentially with energy. Both components have the same energy dependence as background in the data region. Statistics are better, however, since the first time channel covers the total time between beam pulses that is outside the flight time window. The counts per channel in this spectrum were scaled to match the background outside the data loci before being subtracted from the counts within the loci. Overlap of the loci necessitates an additional correction. Counts in the overlap region are divided between loci in the same ratio as the sums of counts between the two pairs of locus limits.

The reaction yield Y is obtained by summing counts corrected for background over several channels. This enhances statistical accuracy, but at the expense of neutron-energy resolution. Two types of sums are used. For a given flight time channel number, counts are summed over all particle energies within the locus limits (horizontally in Fig. 1). For a given energy channel number, counts are summed vertically between the flight time channels limiting the loci. The data are further combined by adding the results of vertical sums for two neighboring channels. Horizontal sums for the first 15 flight time channels are combined in five groups of three channels each and the remaining flight time channels are treated individually. For each of these data subregions the factor $\Delta E_n \Delta E_\alpha$ and the mean energies $\bar{E}_\alpha$ and $\bar{E}_n$ are calculated.[24]

The stopping cross sections used in Eq. (1) were calculated from those for protons in pure boron measured by Overley and Whaling.[26] These were corrected for the α-particle effective charge using the measurements of Armstrong *et al.*[27] The results were divided by the target purity factor to calculate effective stopping cross sections per ^{10}B atom for each target.

Measured incident neutron spectra were not evaluated at energy $\bar{E}_n$, but rather integrated over the interval $\bar{E}_n \pm \Delta E_n/2$, and then divided by ΔE_n. This corrected for nonlinear energy dependences in the spectrum. Although the calculated value of $\bar{\nu}$ is 0.999, zero degree spectra were used ($\bar{\nu} = 1.0$) because the neutron yield does not vary appreciably with angle near zero degrees.

Results of the cross section calculations for both

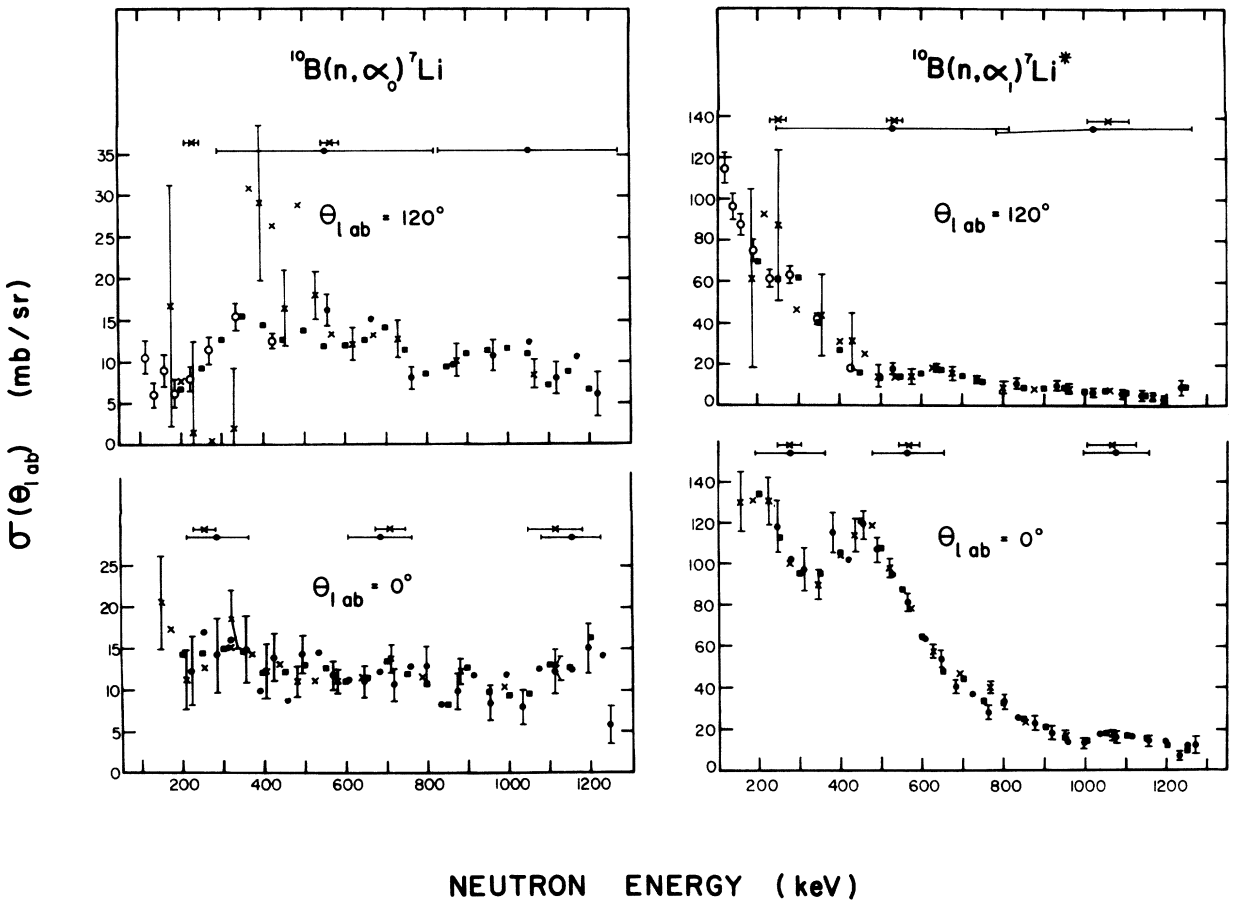

FIG. 2. Differential cross sections calculated from data sets similar to that of Fig. 1. Vertical sums are shown by the dots and horizontal sums by the crosses and open circles. The open circles were obtained from the supplementary run with an 8 cm neutron flight path. The squares are interpolated cross sections at 50 keV intervals. Examples of neutron energy intervals are shown at the top of each graph.

reactions are shown in Fig. 2. The dots are derived from vertical summations while the crosses are from horizontal summations. Since the same yield data were used, results should agree on the average. Where shown, the error bars represent statistical standard deviations. Examples of neutron-energy intervals ΔE_n are plotted above some data points. Cross sections shown by open circles are from horizontal summations for a supplementary back angle run that used an 8 cm flight path.

To obtain angular distributions from excitation functions, cross sections at each angle must be inferred at common energies. Cross sections at 50 keV intervals from 200 to 1250 keV were calculated from a parabola fitted to four data points, the two nearest on each side of a given energy. Results of this process are indicated in Fig. 2 by the squares. The cross section obtained was assigned a standard deviation equal to the average of the standard deviations of the two nearest data points. A weighted mean cross section and its standard deviation were calculated from all interpolated cross sections at the same energy and angle.[28] These were converted to the center of momentum system and combined into angular distributions.

A series of Legendre polynomials was fitted to each angular distribution. Coefficients B_L and their standard deviations were calculated by least squares methods for the expression:

$$\sigma(\mu)=\sum_{L=0}^{K} B_L P_L(\mu) \ . \tag{2}$$

The number of polynomials, $K+1$, was varied from 3 to 5. Three terms proved adequate for all but the 300 to 500 keV neutron-energy range for the first excited state reaction. χ^2 tests showed that four terms best described the α_1 angular distributions for those energies. Examples of angular distributions and Legendre polynomial fits are shown in Fig. 3.

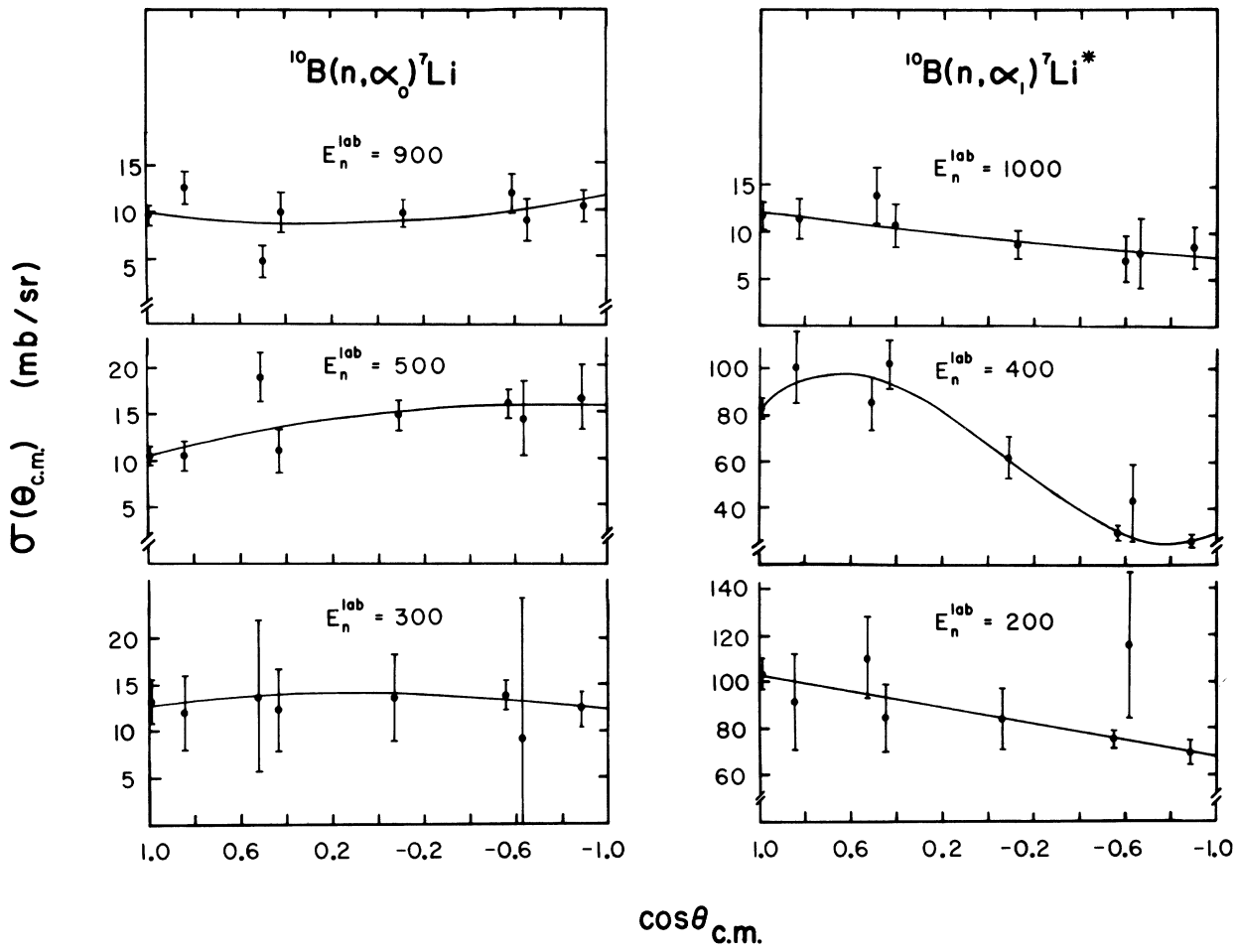

FIG. 3. Angular distributions at several laboratory neutron energies. Error bars represent the statistical yield uncertainties. The curves are calculated from the coefficients of Legendre polynomials obtained in a least squares fit.

IV. UNCERTAINTIES AND ERRORS

The uncertainty of these results can be assessed by considering individually the terms of Eq. (1). Statistical uncertainty in the reaction yield is the largest single source of error and is approximately equal to the quadratic combination of all other uncertainties. There is also uncertainty in the energy and angle to which a cross section is assigned.

The reaction yield and incident neutron flux measurements are sources of statistical uncertainty.

Uncertainty due to counting statistics in the measurement of $I(\bar{E}_n, \bar{\nu})$ varied from 7% below 250 keV to 1% at 1300 keV. Fluctuations in lithium target composition and beam pulse quality limited reproducibility of the neutron flux to ± 3%. When assigning errors to the interpolated cross sections, no allowance was made for the averaging effect of fitting four adjacent data points. It was assumed that this averaging compensated for statistical uncertainty in $I(\bar{E}_n, \bar{\nu})$.

Systematic error can occur in the effective stopping cross section, neutron yield, solid angle convolution, and the area $\Delta E_n \Delta E_\alpha$. Uncertainty in the effective stopping cross section is estimated to be 9%. This results from 4% uncertainty in the proton stopping cross sections for pure ^{10}B,[26] 3% uncertainty in the effective charge corrections,[27] and 8% uncertainty in the target purity factor. The target purity studies combined proton stopping cross sections in Li, F, and B and the determinations of peak widths. These stopping cross sections were known to about 4% and widths were determined to within 3%. Neglecting the relatively small uncertainties in ^6Li and ^{10}B thermal neutron cross sections and counting statistics, the purity factor is known to ±8%.

Systematic errors in the neutron yield arise from a 5% uncertainty in the zero degree yield

of Burke *et al.*,[25] and error in matching their detector bias. When combined these sources yield 6% uncertainty at 200 keV and 5% at the highest energies. Since Burke obtained detector efficiencies through normalization to the absolute $^7Li(p,n)^7Be$ cross section measurements of Macklin and Gibbons,[29] the present results will reflect any systematic errors in those measurements.

Both the solid angle convolution, $\Delta\Omega$, and the area $\Delta E_n \Delta E_\alpha$ were corrected for extended geometry to better than 1% by the techniques of Ref. 24. Measuring target and detector radii and flight paths to 1% results in a 4% uncertainty in $\Delta\Omega$. Systematic error in $\Delta E_n \Delta E_\alpha$ is estimated to be less than 4% over the entire energy range. For purposes of estimating uncertainty the area is approximated as a product of a neutron energy interval and an α-particle energy interval. Each interval is known to about 3% on the basis of target thickness and time scale uncertainties.[23]

Other sources of error are scattered neutrons, charge integration, and calibrations. Since the detector shield was a source of scattered neutrons, neutron yield measurements were made with the shield in place. They were within 1% of measurements without the shield. Events due to neutrons scattered from more distant objects were excluded from the data region by their long flight times. Charge integrations for data collection and yield measurements were corrected for electronic dead times and are believed to be accurate to 0.1%. The slope and intercept of the linear flight time scale were determined to 1%. The pulser calibra-

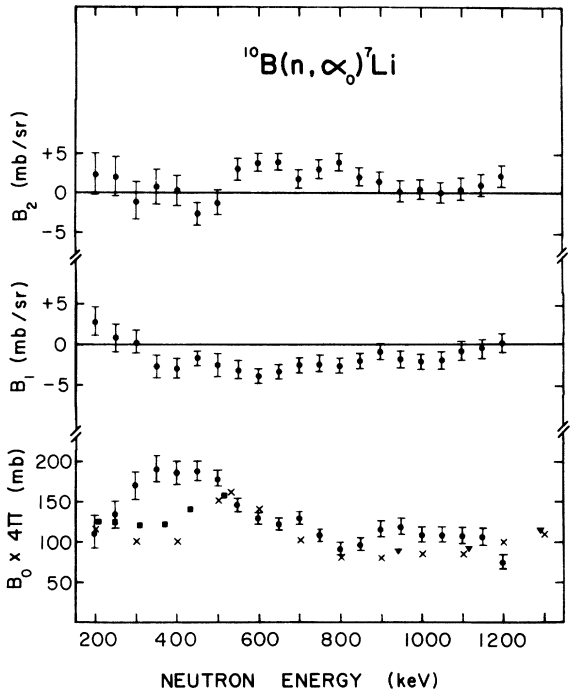

FIG. 4. Coefficients of Legendre polynomials from a least squares fit to c.m. angular distributions for the $^{10}B(n,\alpha_0)^7Li$ reaction. The error bars were calculated from statistical yield uncertainties. Other integrated cross section measurements are those of Davis *et al.* (Ref. 11) (crosses), Macklin and Gibbons (Ref. 10) (squares), and Van der Zwan and Geiger (Ref. 17) (inverted triangles).

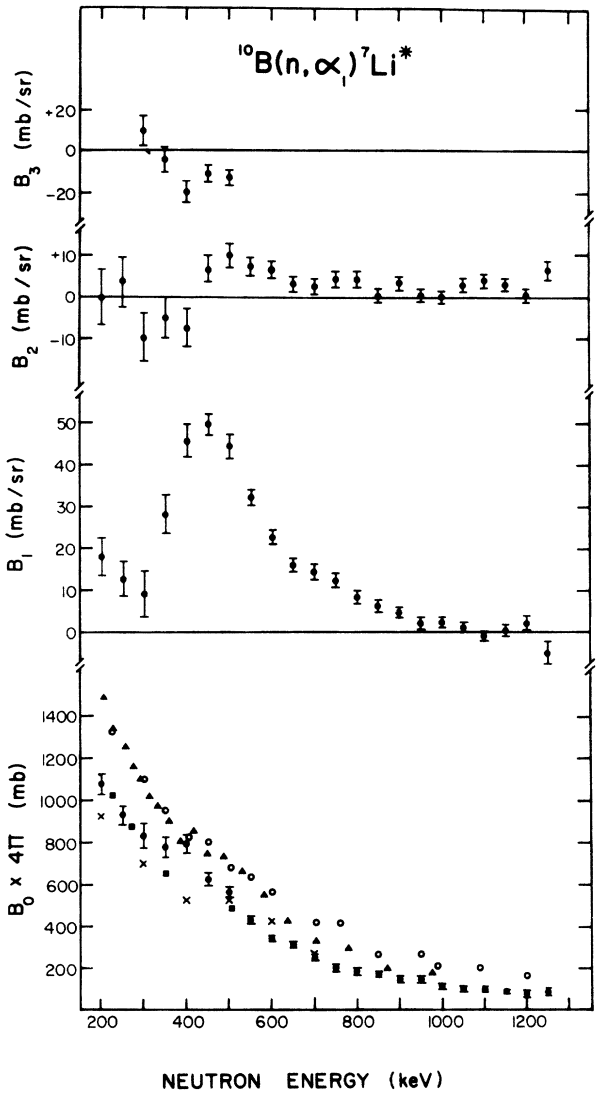

FIG. 5. Coefficients of Legendre polynomials from a least squares fit to c.m. angular distributions for the $^{10}B(n,\alpha_1)^7Li^*$ reaction. The error bars were calculated from statistical yield uncertainties. Other integrated cross section measurements are those of Davis *et al.* (Ref. 11) (crosses), Macklin and Gibbons (Ref. 10) (squares), Friesenhahn *et al.* (Ref. 9) (triangles), and Nellis *et al.* (Ref. 12) (open circles).

tion was accurate to 0.5%. Centroids of the energy calibration peaks were reproduced by the linear energy scale to within ±4 keV in the range from 1 to 3 MeV.

These cross sections represent averages over intervals of energy and angle. They are subject to error in the mean reaction angle cosine $\bar{\mu}$ and the center of the neutron energy interval $\bar{E}_n$. As a worst case example of angular resolution, for a nominal reaction angle of 55° the calculated mean and standard deviation were 55.1°± 4.5°. Reaction angle cosines and their standard deviations were corrected for extended geometry to better than 1%. Uncertainty in $\bar{E}_n$ is of the order of a few percent. Since most of the cross sections vary smoothly with energy, these errors are unimportant.

When all errors except the statistical yield uncertainty are quadratically combined a ±12% overall systematic uncertainty results.

V. RESULTS AND CONCLUSIONS

Coefficients in the Legendre polynomial expansion for both reactions are plotted against laboratory neutron energy in Figs. 4 (α_0) and 5 (α_1). The error bars shown were calculated from the statistical yield uncertainties of the input data. Values of the coefficients and their standard deviations are presented in Table I. In Fig. 4, Fig. 5, and Table I integrated cross sections $4\pi B_0$ are presented rather than B_0. Figures 4 and 5 also contain other measurements of the integrated cross sections. Absorption cross sections (approximated as sums of α_0 and α_1 integrated cross sections) and branching ratios can be calculated from the data in Table I.

The overall uncertainty of integrated cross sections deduced from our results is too large to resolve discrepancies among other measurements. For the ground state cross sections there are no significant disagreements with other works except for a broad peak between 300 and 450 keV. This peak is seen most clearly in the supplementary data at 120° and 150° (note the open circles in the 120° α_0 data of Fig. 2). Although Lane *et al.*[19] found a peak at 370 keV in neutron elastic scattering from ^{10}B, they assigned it a negligible ground state α-particle partial width because similar structure had not been seen in ^{7}Li$(\alpha,n)^{10}$B (Ref. 10). We have begun a measurement of ^{7}Li$(\alpha,n)^{10}$B differential cross sections using thick target techniques to investigate this discrepancy.

The present measurements of the first excited state integrated cross section show a mixed agreement with other data. Above 600 keV they support the measurements of Davis *et al.*[11] Davis's results above 800 keV are not plotted in Fig. 5 be-

TABLE I. Coefficients of Legendre polynomials from a least squares fit to the c.m. angular distributions. Standard deviations were calculated from the statistical yield uncertainties.

	$^{10}B(n, \alpha_0)^7$Li			$^{10}B(n, \alpha_1)^7$Li*			
E_n (lab) (keV)	$4\pi B_0$ (mb)	B_1 (mb/sr)	B_2 (mb/sr)	$4\pi B_0$ (mb)	B_1 (mb/sr)	B_2 (mb/sr)	B_3 (mb/sr)
200	113.0± 17.7	2.9± 1.7	2.3± 2.5	1091± 48	17.9± 4.4	0.0± 6.6	
250	136.1± 17.6	0.8± 1.7	2.1± 2.5	947± 45	12.9± 4.0	3.7± 6.0	
300	172.4± 17.2	0.2± 1.5	1.0± 2.3	850± 58	9.5± 5.4	−9.9± 5.8	9.7± 7.1
350	193.5± 16.6	−2.8± 1.4	0.8± 2.2	791± 48	28.5± 4.4	−4.9± 5.0	− 4.4± 5.7
400	186.0± 12.3	−3.0± 1.2	0.5± 1.8	808± 43	46.4± 4.0	−7.5± 4.4	−19.9± 5.2
450	182.3± 10.2	−1.5± 0.9	−1.9± 1.4	640± 28	50.3± 2.6	6.9± 2.9	−10.8± 3.2
500	182.8± 9.4	−3.0± 0.9	0.9± 1.3	577± 21	45.4± 2.7	10.3± 2.8	−12.8± 3.9
550	148.9± 7.3	−3.2± 0.8	2.8± 1.0	441± 15	32.7± 1.7	7.5± 2.1	
600	131.3± 6.9	−4.0± 0.8	3.9± 1.0	349± 14	23.0± 1.5	6.9± 1.9	
650	124.7± 6.9	−3.4± 0.8	3.9± 1.0	322± 12	16.3± 1.5	3.6± 1.8	
700	131.7± 7.7	−2.7± 0.9	1.8± 1.1	258± 12	14.5± 1.6	2.9± 1.8	
750	110.0± 7.5	−2.4± 0.9	3.1± 1.1	212± 12	12.3± 1.6	4.6± 1.8	
800	93.5± 7.4	−2.7± 0.9	4.0± 1.0	192± 11	8.4± 1.5	4.5± 1.7	
850	99.3± 8.2	−2.0± 0.9	2.1± 1.1	179± 11	6.1± 1.5	0.6± 1.7	
900	118.5± 8.7	−0.8± 0.9	1.5± 1.2	153± 12	4.7± 1.4	3.6± 1.7	
950	121.5± 9.7	−1.9± 1.0	0.3± 1.3	150± 11	2.0± 1.4	0.6± 1.6	
1000	111.8± 8.7	−2.2± 1.0	0.5± 1.2	122± 10	2.4± 1.2	0.2± 1.5	
1050	112.1± 9.0	−2.1± 1.1	0.1± 1.2	108± 10	1.1± 1.3	3.1± 1.5	
1100	114.6± 9.9	−1.1± 1.0	0.5± 1.3	103± 10	−1.0± 1.4	4.2± 1.5	
1150	109.0± 9.3	−0.4± 1.0	1.1± 1.3	91.5± 9.0	0.3± 1.3	3.2± 1.4	
1200	76.9± 8.4	0.3± 1.2	2.3± 1.3	84.3± 11.3	2.2± 1.6	0.6± 1.7	
1250				90.0± 15.5	−5.1± 2.6	6.8± 2.2	

cause they overlap the present results. Below 600 keV our measurements lie between the extremes of Davis *et al.*[11] and Nellis *et al.*[12] The shoulder at 400 keV is consistent with structure seen in the integrated α_1 and absorption cross sections of Friesenhahn *et al.*[9] and with the state at 370 keV found by Lane *et al.*[19]

Analysis of preliminary data showed that the (n,α_1) angular distributions were strongly forward peaked over most of the energy range. This contradicted the assumption of Lane *et al.*[19] that only s-wave neutrons contribute to the α_1 reactions below 1 MeV, leading to isotropic angular distributions.[21] Therefore, in a subsequent paper[30] they modified their parameters, placing about half the α-particle partial width of a previously parametrized p-wave state at 530 keV in the α_1 channel. Since this change invalidates the predictions of Ref. 21, they have not been included in Figs. 4 and 5. Predictions based on the new parameters are not available.

More extensive R-matrix work on the ^{11}B system is underway at Los Alamos.[20] The present results are being included in those calculations.

In the absence of definitive R-matrix results, only qualitative features of ^{11}B level structure can be inferred from Figs. 4 and 5. Coefficients of P_1 indicate that the p-wave state at 530 keV interferes with s-wave states in both α-particle channels over an 800 keV wide neutron energy interval. From 300 to 500 keV fits to the α_1 angular distributions were improved by adding a fourth term. These nonzero coefficients of P_3 suggest the presence of a d-wave state that is interfering with the p-wave state at 530 keV. A possible source of d-wave strength is a state at an excitation energy of 11.46 MeV for which Hale[20] postulated $J^{\pi} = \frac{3}{2}^{+}$.

ACKNOWLEDGMENTS

We would like to acknowledge helpful discussions with Professor R. O. Lane and Dr. G. M. Hale. Dr. D. H. Ehlers contributed to the early stages of this experiment. M. Karim and G. Yu assisted in the data collection. W. Schultz and J. D. MacDonald maintained the equipment. We also appreciate the critical interest shown in this work by Professor H. W. Lefevre.

---

†Work supported in part by the National Science Foundation.

[1]F. Ajzenberg-Selove and T. Lauritsen, Nucl. Phys. A114, 1 (1968).

[2]Cross sections for thermal neutrons were calculated from those reported by J. W. Meadows, in *Neutron Standards and Flux Normalization*, proceedings of a Conference at Argonne, 1971 (National Technical Information Service, Springfield, Virginia 1971), CONF-701002, p. 129, using the branching ratio of Macklin and Gibbons (Ref. 10).

[3]H. Bichsel and T. W. Bonner, Phys. Rev. 108, 1025 (1957).

[4]S. A. Cox and F. R. Pontet, J. Nucl. Energ. 21, 271 (1967).

[5]B. Petree, C. H. Johnson, and D. W. Miller, Phys. Rev. 83, 1148 (1951).

[6]F. P. Mooring, J. E. Monahan, and C. M. Huddleston, Nucl. Phys. 82, 16 (1966).

[7]D. Bogart and L. L. Nichols, Nucl. Phys. A125, 463 (1969).

[8]M. G. Sowerby, B. H. Patrick, C. A. Uttley, and K. M. Diment, J. Nucl. Energ. 24, 323 (1970).

[9]S. J. Friesenhahn, V. J. Orphan, A. D. Carlson, M. P. Fricke, and W. M. Lopez, USAEC Report No. INTEL RT 7011-001, 1974 (unpublished).

[10]R. L. Macklin and J. H. Gibbons, Phys. Rev. 165, 1147 (1968).

[11]E. A. Davis, F. Gabbard, T. W. Bonner, and R. Bass, Nucl. Phys. 27, 448 (1961).

[12]D. O. Nellis, W. E. Tucker, and I. L. Morgan, Phys. Rev. C 1, 847 (1970).

[13]R. L. Macklin and J. H. Gibbons, Phys. Rev. 140, 324 (1965).

[14]M. G. Sowerby, J. Nucl. Energ. 20, 135 (1966).

[15]A. J. Deruytter and P. Pelfer, J. Nucl. Energ. 21, 833 (1967).

[16]G. P. Lamaze, A. D. Carlson, and M. M. Meier, Nucl. Sci. Eng. 56, 94 (1975).

[17]L. Van der Zwan and K. W. Geiger, Nucl. Phys. A180, 615 (1972).

[18]R. Y. Cusson, Nucl. Phys. 86, 481 (1966).

[19]R. O. Lane, S. L. Hausladen, J. E. Monahan, A. J. Elwyn, F. P. Mooring, and A. Langsdorf, Jr., Phys. Rev. C 4, 380 (1971).

[20]G. M. Hale, in *Proceedings of the Conference on Nuclear Cross Sections and Technology*, edited by C. D. Bowman and R. A. Schrack (National Bureau of Standards, Washington, D. C. 1975).

[21]S. L. Hausladen, R. O. Lane, and J. E. Monahan, Phys. Rev. C 5, 277 (1972).

[22]R. M. Sealock and J. C. Overley, Bull. Am. Phys. Soc. 17, 900 (1972).

[23]J. C. Overley, R. M. Sealock, and D. H. Ehlers, Nucl. Phys. A221, 573 (1974).

[24]J. C. Overley and D. H. Ehlers, Nucl. Instrum. 111, 13 (1973).

[25]C. A. Burke, M. T. Lunnon, and H. W. Lefevre, Phys. Rev. C 10, 1299 (1974).

[26]J. C. Overley and W. Whaling, Phys. Rev. 128, 315 (1962).

[27]J. C. Armstrong, J. V. Mullendore, W. R. Harris, and J. B. Marion, Proc. Phys. Soc. (London) 86, 1283 (1965).

[28]Laboratory differential cross sections and statistical standard deviations at 22 neutron energies and 8 angles have been sent to the National Neutron Cross Section Center, Brookhaven National Laboratory.

[29]R. L. Macklin and J. H. Gibbons, Phys. Rev. 109, 105 (1958); J. H. Gibbons and R. L. Macklin, *ibid*. 114, 571 (1959); R. L. Macklin, private communication to H. Lefevre.

[30]S. L. Hausladen, C. E. Nelson, and R. O. Lane, Nucl. Phys. A217, 563 (1973).